28. INTERSTITIAL-WATER STUDIES OF SAMPLES FROM THE PASSIVE GALICIA MARGIN, NORTHEAST ATLANTIC, OCEAN DRILLING PROGRAM LEG 103[1]

Janet A. Haggerty, Department of Geosciences, University of Tulsa, Tulsa, Oklahoma
and
J. Berton Fisher, Amoco Production Company, Tulsa Research Center, Tulsa, Oklahoma

ABSTRACT

Interstitial waters were squeezed from strata recovered at Sites 637–641 of ODP Leg 103 on the Galicia margin, along the northwestern Iberian continental margin in the northeast Atlantic. Chemical profiles of Site 638 show the most complexity, which appears to be related to an unconformity in the strata between Cretaceous and Neogene sediments and to rapid deposition of Cretaceous syn-rift sediments upon pre-rift strata. Analyses of waters from all of the Leg 103 sites show generally antithetical trends for calcium and magnesium; calcium increases with depth as magnesium decreases. No calcium-magnesium "crossover" profiles are observed in these data. Data from Site 637 show an unusual pattern; calcium increases with increasing depth, but magnesium remains relatively constant. Sulfate is either stable or shows an overall decrease with depth, and boron profiles show some structure. At all but one site (Site 638), strontium profiles do not show marked depth structure. The structure of alkalinity and silica profiles is highly site dependent. Bromide profiles are, in general, constant. In nearly every case, observed bromide concentrations are near average seawater values. Relatively low concentrations of iron and manganese are common within the upper 10 m of the sediment sequence and typically are near detection limits at deeper depths.

INTRODUCTION

Leg 103 of the Ocean Drilling Program (ODP) sampled the Galicia margin along the northwest region of the Iberian Peninsula (Figs. 1A and 1B). A transect of five sites (Fig. 1C) was drilled along this sediment-starved passive margin for the purpose of determining the tectonic evolution of the region from pre- through post-rift stages. A composite stratigraphic column of the strata recovered on Leg 103 is presented in Figure 1D. Drilling at Site 639 penetrated dolomite and limestone from a carbonate platform interpreted as pre-rift strata (see "Site 639" chapter; Shipboard Scientific Party, 1987c). Syn-rift strata containing turbidites were recovered at Sites 638 and 641 (see "Site 638" and "Site 641" chapters; Shipboard Scientific Party, 1987b, 1987d). The syn-rift strata at Site 641 are overlain by hemipelagic sediments interpreted as post-rift strata. Site 637 penetrated through post- and syn-rift sediments into peridotite basement that is interpreted to be mantle-derived material emplaced during rifting (see "Site 637" chapter; Shipboard Scientific Party, 1987a). Site 640 was drilled to determine if the S reflector is a boundary surface between brittle and ductile continental basement or if it is an acoustic impedance contrast between different sedimentary rocks or between sediment and crystalline basement. Primarily syn-rift sediments were recovered at Site 640. Interstitial waters from the strata recovered on Leg 103 were analyzed to reveal diagenetic rock–pore water interactions.

METHODS

Sediment samples from cores recovered at each site were squeezed aboard ship for interstitial waters. Shipboard analyses were made for pH, alkalinity, calcium, magnesium, chlorinity, and salinity. Semiautomatic titration using a Metrohm titrator was used for the pH and alkalinity analyses. Titrations were used for analysis of calcium, magnesium, and chloride following the procedures of Gieskes (1974; Salisbury, Scott, et al., 1987). Salinity was determined using a Goldberg refractometer. These data are reported in the site chapters in the *Initial Reports* of the Leg 103 *Proceedings* (Boillot, Winterer, et al., 1987).

All other data were obtained by onshore laboratory analysis of interstitial-water samples. Sodium, calcium, magnesium, strontium, manganese, iron, boron, and silica data were determined by inductively coupled plasma atomic emission spectroscopy (ICP-AES) using an Applied Research Laboratories Model 3510 instrument. Bromide, sulfate, and chloride data were determined by ion chromatography (IC) using an Dionex Model 2000i instrument.

During shipment of the interstitial-water samples from port call in Germany to the senior author, more than one-third of the samples were destroyed. Consequently, additional samples were requested from the ODP Repository in College Station, Texas. Neither a complete set of field-acidified (titrated for alkalinity) samples nor a complete set of unacidified samples could be obtained from the repository. These complications, which were compounded by small sample size and differences in evaporative concentration, resulted in the use of ICP-AES and IC methodologies and the application of evaporation correction and normalization between treatment types to the laboratory data, as detailed in the following.

In general, ICP-AES analyses were performed on field-acidified (titrated for alkalinity) samples. Exceptions were sodium, which was measured on both acidified and unacidified samples, and calcium and magnesium, which were determined for an unacidified sample if an aliquot of the acidified sample was not available. Standards and samples for ICP-AES analysis were prepared using HCl as a diluent. All IC analyses were conducted on unacidified samples using deionized (ASTM Type III) water as a diluent. The precision of both ICP-AES and IC analyses is better than 5% (rsd). Based on comparison of shipboard and laboratory measurements of chloride, magnesium, and calcium, charge-balance calculations (see the following), and repeated measurements of standard materials, the accuracy of both ICP-AES and IC analyses is typically better than 2%–5%, but exceeds 10% in rare instances.

As a consequence of differences in evaporative concentration and dilution (acid addition) among samples and between treatments (acidified and unacidified), the results of the laboratory measurements required normalization. Correction for evaporative concentration and dilution was achieved by making a ratio of the field-determined calcium and magnesium to the laboratory-determined values for these parameters. In the case of the unacidified samples, the ratio of field-determined chlorinity to laboratory-determined chloride was also used. For the acidified samples, evaporation or dilution correction was accomplished by multiplying the laboratory-determined value by the average of Ca_{field}/Ca_{lab}

---

[1] Boillot, G., Winterer, E. L., et al., 1988. *Proc. ODP, Sci. Results*, 103: College Station, TX (Ocean Drilling Program).

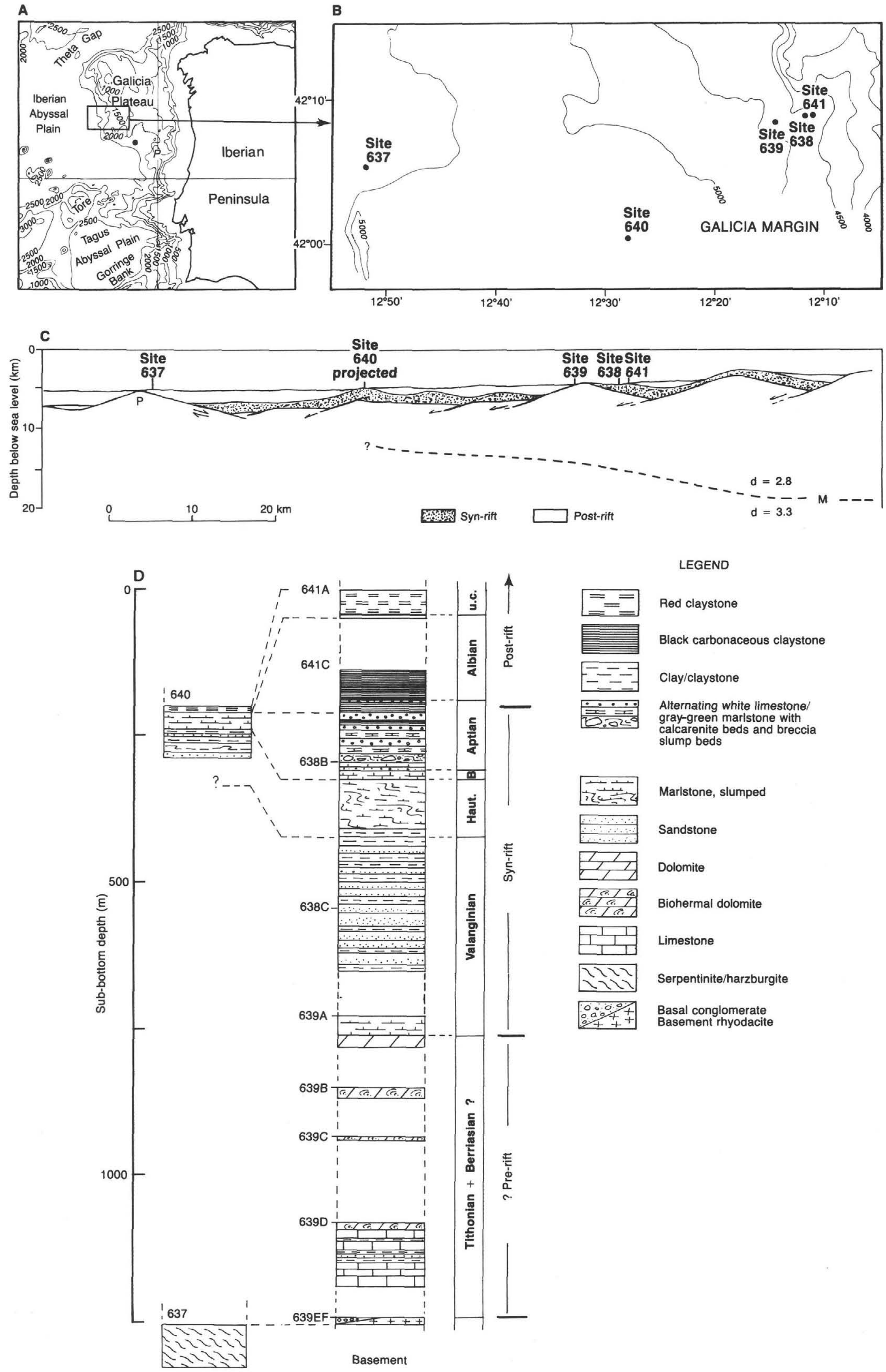

Figure 1. **A.** Leg 103 drilled on the western Galicia margin along the northwest Iberian Peninsula. **B.** Location of the Leg 103 drill sites. **C.** Schematic cross section of the Galicia margin displaying the transect of the five drill sites. S = deep seismic reflector; P = peridotite ridge. **D.** Composite stratigraphic column for the Galicia margin assembled from lithologies recovered at each drill site.

or Mg_{field}/Mg_{lab}. For the unacidified samples, evaporation correction was made by multiplying the laboratory-determined value by the average of the most consistent (i.e., showing the smallest difference) pair among the Cl_{field}/Cl_{lab}, Ca_{field}/Ca_{lab}, and Mg_{field}/Mg_{lab} ratios. The evaporation or dilution correction factors are quite consistent. Of the 44 samples examined, only 13 show differences in excess of 0.05 in the ratios used, and of these, only two show a difference of more than 0.10. Normalization of data between acidified and unacidified treatments (when necessary) was accomplished by making a ratio of the Na concentrations measured for the two treatments. The most complicated correction required both evaporation correction and normalization between treatment types. For example, the normalized and evaporation-corrected value for an ion measured in an unacidified sample for which calcium and magnesium data were available only for the acidified sample would be calculated by:

$$C(N) = [Ke \times Na(A)]/[Na(U) \times C(U)],$$

where C(N) is the normalized and evaporation-corrected concentration of the ion, C(U) is the concentration of the ion in the unacidified sample, Ke is the correction factor for evaporation, and Na(A) and Na(U) are, respectively, the sodium concentration in the acidified and unacidified samples. The data used for evaporation correction and normalization are given in Table 1. All laboratory data (with the exception of chloride, calcium, and magnesium, which were measured solely for evaporation and dilution correction) are given in Table 2. These data have been corrected and normalized. Notations in Table 2 indicate data items omitted from consideration because of poor accuracy.

Following the evaporation correction and normalization calculation, a charge-balance calculation was performed based on the abundance of major anions (chloride, sulfate, and bicarbonate) and cations (sodium, calcium, and magnesium). For purposes of the charge-balance calculation, the shipboard alkalinity data were assumed to equal bicarbonate. The charge-balance calculation was made to validate the internal consistency of the data. With few exceptions, the charge-balance calculations indicated internally consistent data. The results of the charge-balance calculations are given in Table 1.

RESULTS AND DISCUSSION

Site 637 (Fig. 2)

Locality Description

Site 637 was drilled into serpentinized peridotite basement lying beneath an approximately 212-m-thick cover of Neogene clay and turbidite sands. The drill site is on a north-trending

Table 1. Correction, normalization, and charge-balance data. Correction factor data: A = Cl_{field}/Cl_{lab}; B = Mg_{field}/Mg_{lab}; C = Ca_{field}/Ca_{lab}; Av. = average of B and C or of the two most consistent ratios if A was available. Charge balance is defined as 100 × [(P − N)/(P + N)], where P = total positive charge and N = total negative charge.

Sample	Depth (mbsf)	Correction factor data				Na		Charge balance (%)
		A	B	C	Av.	unacidified (mmol/L)	acidified (mmol/L)	
103-637A-6R-2, 140–150 cm	47.8	0.95	0.92	0.97	0.94	515.6	542.5	1.40
7R-2, 140–150 cm	57.9	0.75	0.73	1.49	0.74	651.6		−1.02
9R-1, 140–150 cm	75.4	0.92	0.85	0.86	0.86	556.6		2.63
15R-3, 140–150 cm	136.1	0.96	0.87	0.96	0.96	552.9		3.80
18R-3, 140–150 cm	162.1	0.97	0.89	0.89	0.89	507.4		0.30
23R-3, 0–10 cm	211.8		0.36	0.44	0.40		3223.6	47.32
103-638B-1R-2, 140–150 cm	2.9	0.99	0.97	0.97	0.97	478.4	491.5	0.76
2R-4, 140–150 cm	12.3	1.04	0.99	1.00	1.00	472.5	3302.1	−1.28
3R-1, 140–150 cm	17.4	0.84	1.02	1.04	1.03	588.7	457.2	−2.14
4R-4, 140–150 cm	31.4	0.92	0.87	0.92	0.92	535.6	14741.7	0.14
7R-1, 140–150 cm	55.8	1.00	0.84	0.92	0.88	488.1	579.6	0.97
11R-2, 140–150 cm	96.6	0.86	0.91	0.99	0.95	579.3	530.3	0.88
14R-2, 140–150 cm	125.8		0.97	1.01	0.99	509.7	509.7	6.43
18R-4, 140–150 cm	167.4	0.82	0.81	0.92	0.81	563.4	18220.0	−0.53
21R-3, 140–150 cm	194.5	0.51	0.91	0.94	0.92	777.5	603.5	9.48
24R-5, 140–150 cm	226.2		0.99	1.02	1.00		526.5	9.65
26R-5, 140–150 cm	245.5	0.83	0.86	0.92	0.89	560.2	586.3	2.36
29R-2, 140–150 cm	269.9	0.75	1.01	1.04	1.02	522.1	536.6	9.86
32R-1, 140–150 cm	297.4	0.89	0.90	0.97	0.94	487.5	542.1	1.00
35R-3, 140–150 cm	329.3		0.75	0.79	0.77		710.9	11.83
45R-2, 140–150 cm	424.4	0.70	0.80	0.94	0.75	573.8		−0.58
103-683C-4R-2, 140–150 cm	443.8	0.51	0.96	1.00	0.98		523.6	5.45
7R-2, 140–150 cm	472.8	0.61	0.62	0.68	0.61	797.5		−1.40
10R-1, 140–150 cm	500.3	1.17	0.86	0.94	0.90	556.0		0.22
103-639A-1R-4, 140–150 cm	2.0	1.28	1.08	0.99	1.03	524.4	479.0	1.46
2R-3, 140–150 cm	6.7	0.96	0.99	0.98	0.98	607.6	529.5	2.73
3R-2, 140–150 cm	14.9	1.01	0.84	1.05	1.03	551.6		7.41
5R-1, 140–150 cm	33.3	0.92	1.02	0.98	1.00	604.1	524.1	3.02
6R-1, 140–150 cm	43.0	0.73	1.00	0.97	0.99		532.0	10.28
7R-1, 140–150 cm	52.6	0.15	1.02	0.99	1.01		493.9	6.89
103-639B-1R-1, 0–10 cm	0.0	1.28	1.05	1.04	1.05	490.3	512.7	3.97
1R-5, 140–150 cm	7.4	1.15	1.04	1.03	1.03	504.2	479.1	2.08
103-640A-3R-2, 140–150 cm	167.7	0.97	0.92	0.78	0.85	568.3	577.5	2.19
7R-1, 140–150 cm	204.7	1.24	0.79	0.83	0.81	477.0	631.0	3.72
103-641A-1X-2, 140–150 cm	2.9	0.93	0.83	0.87	0.85	492.7	569.6	1.50
2X-3, 140–150 cm	10.5	0.98	0.94	0.91	0.92	513.5		−0.47
3X-1, 140–150 cm	17.1	0.57	0.63	0.65	0.64	749.6		−0.17
5X-2, 140–150 cm	37.8	0.83	1.00	0.97	0.98	496.8	463.8	0.26
7X-4, 140–150 cm	60.0	0.67	0.82	0.80	0.81	591.2		4.29
103-641C-3R-6, 140–150 cm	169.4	0.91	1.07	1.09	1.08	554.6	447.4	3.18
6R-2, 140–150 cm	207.9	1.35	0.66	0.70	0.68	476.0	506.7	−9.30
8R-1, 140–150 cm	219.8	0.61	0.96	0.99	0.98		513.8	11.10
11R-4, 140–150 cm	253.2	1.05	0.85	0.88	0.87	512.4	618.4	14.95
14R-2, 140–150 cm	279.1	1.00	1.02	1.00	1.01	608.5	474.2	1.11

Table 2. Corrected and normalized laboratory data for Leg 103.

		Evaporation/dilution corrected and normalized chemical data							
Sample	Depth (mbsf)	Na (mmol/L)	Sr (mmol/L)	Br (mmol/L)	SO_4 (mmol/L)	SiO_2 (mmol/L)	B (mmol/L)	Fe (mmol/L)	Mn (mmol/L)
103-637A-6R-2, 140–150 cm	47.8	511	0.09	0.76	20.47	0.59	0.62	0.00	0.00
7R-2, 140–150 cm	57.9	483	0.04	0.74	18.02	1.08	0.42		
9R-1, 140–150 cm	75.4	478	0.09	0.78	16.01	0.50	0.62		
15R-3, 140–150 cm	136.1	529	0.12	0.80	19.97	0.40	0.59		
18R-3, 140–150 cm	162.1	452	0.12	0.68	19.46	0.45	0.69		
[a]23R-3, 0–10 cm	211.8	1295						0.00	0.00
103-638B-1R-2, 140–150 cm	2.9	476	0.09	0.73	30.17	0.50	0.56	0.01	0.01
2R-4, 140–150 cm	12.3	472	0.14	0.74	28.93	0.55	0.53		
3R-1, 140–150 cm	17.4	471	0.16	0.74	28.45	0.56	0.48	0.00	0.00
4R-4, 140–150 cm	31.4	494	0.21	0.80	27.90	0.38	0.49		
7R-1, 140–150 cm	55.8	509	0.35	0.86	28.22	0.82	0.52	0.00	0.00
11R-2, 140–150 cm	96.6	503	0.39	0.81	25.38	0.43	0.46	0.00	0.00
14R-2, 140–150 cm	125.8	505	0.31			0.29	1.01	0.00	0.00
18R-4, 140–150 cm	167.4	459	0.35	0.73	21.95	0.90	0.42		
21R-3, 140–150 cm	194.5	557	0.35	0.87	33.45	0.61	0.50	0.00	0.00
24R-5, 140–150 cm	226.2	527						0.00	0.00
26R-5, 140–150 cm	245.5	522	0.31	0.89	29.17	0.73	0.67	0.00	0.00
29R-2, 140–150 cm	269.9	548	0.26	0.89	30.45	1.66	0.64	0.00	0.00
32R-1, 140–150 cm	297.4	507	0.24	0.84	29.66	0.97	0.63	0.00	0.00
[a]35R-3, 140–150 cm	329.3	548						0.00	0.00
[b]45R-2, 140–150 cm	424.4	431	0.15	0.73	25.17	0.66	0.51		
103-638C-4R-2, 140–150 cm	443.8	514	0.19			0.21	0.95	0.01	0.00
7R-2, 140–150 cm	472.8	489	0.12	0.75	29.34	1.18	0.44		
10R-1, 140–150 cm	500.3	501	0.15	0.76	26.14	1.21	0.50		
103-639A-1R-4, 140–150 cm	2.0	496	0.08	0.73	29.43	0.71	0.58	0.10	0.06
2R-3, 140–150 cm	6.7	521	0.08	0.77	33.16	0.56	0.47	0.01	0.05
3R-2, 140–150 cm	14.9	570	0.08	0.94	34.07	1.49	0.55		
5R-1, 140–150 cm	33.3	524	0.08	0.78	31.56	0.52	0.44	0.00	0.00
[a]6R-1, 140–150 cm	43.0	524	0.09			0.46	0.64	0.00	0.00
7R-1, 140–150 cm	52.6	498	0.10			0.47	0.79	0.04	0.00
103-639B-1R-1, 0–10 cm	0.0	536	0.10	0.86	32.09	0.86	0.55	0.01	0.08
1R-5, 140–150 cm	7.4	494	0.08	0.81	28.44	0.65	0.62	0.04	0.04
[b]103-640A-3R-2, 140–150 cm	167.7	492	0.28	0.81	20.52	0.62	0.66	0.00	0.00
7R-1, 140–150 cm	204.7	511	0.36	0.79	16.77	0.67	0.75	0.00	0.00
103-641A-1X-2, 140–150 cm	2.9	484	0.09	0.78	31.89	0.45	0.86	0.00	0.06
2X-3, 140–150 cm	10.5	475	0.08	0.68	31.92	0.78	0.66		
3X-1, 140–150 cm	17.1	479	0.07	0.85	33.42	0.41	0.70		
5X-2, 140–150 cm	37.8	456	0.12	0.72	30.88	0.98	0.73	0.00	0.10
7X-4, 140–150 cm	60.0	477	0.11	0.74	31.93	1.13	0.56		
103-641C-3R-6, 140–150 cm	169.4	483	0.17	0.75	26.98	1.34	0.29	0.00	0.02
6R-2, 140–150 cm	207.9	345	0.15	0.51	16.61	1.20	0.29	0.00	0.05
8R-1, 140–150 cm	219.8	502	0.22			0.61	0.77	0.00	0.01
11R-4, 140–150 cm	253.2	537	0.27	0.80	21.69	0.91	0.40	0.00	0.03
14R-2, 140–150 cm	279.1	480	0.29	0.71	21.54	1.30	0.38	0.02	0.00

[a] Na value questionable because of poor charge balance.

[b] All chemical data questionable because of poor correspondence of evaporation/dilution correction factors.

ridge, approximately 50 km in length, and is situated close to the ocean/continent boundary near the base of the Galicia margin. Unconsolidated sediments sampled for interstitial water at this site are from a nearly continuous section of marls, terrigenous turbidites, and slumped brown clay (lithologic Units I and II), ranging in age from late Miocene through late Pleistocene, that overlie 32.1 m of unfossiliferous red clay (lithologic Unit III). The deepest interstitial-water sample was taken from the uppermost part of the serpentinized peridotite (lithologic Unit IV).

Chemical Profiles

Alkalinity shows an overall decrease with increasing depth below seafloor. Chlorinity decreases slightly. Calcium exhibits a stable to decreasing trend to 75.4 m below seafloor (mbsf) (Unit I) but shows a distinct increase with depth below this point. Unit I is characterized by the highest alkalinity values and by calcium concentrations that are less than that of the overlying seawater, which may be the result of calcium carbonate precipitating from the production of bicarbonate ions during the sulfate reduction process (Gieskes, 1975). Magnesium concentrations show a slight decrease with depth.

Stable profiles are observed for strontium, boron, silica, and bromide. It should be noted, however, that the silica profile contains one excursion (at 57.9 mbsf), with a concentration approximately twice that observed for all other samples from this site. Bromide concentrations observed at this site are only slightly below average seawater values (0.8 mmol/L).

The sulfate profile at this site is remarkable in that it shows a trend reversal. Sulfate decreases to 16.01 mmol/L at a depth of 75.4 mbsf, within the rapidly deposited upper Pliocene–Pleistocene sediments of Unit I, and then increases in the slumped brown clay of Unit II. Gieskes (1981, 1983) suggested that such a pattern may result from more reactive organic matter associated with higher sedimentation rates in the overlying sediments in comparison with the underlying sediments. At Site 637, the rapidly deposited sediments of Unit I (with abundant terrigenous turbidites) contain more organic carbon than the underlying sediments from Unit II. Sediments from Unit II are extremely lean in organic carbon (approximately 0.1%; see "Or-

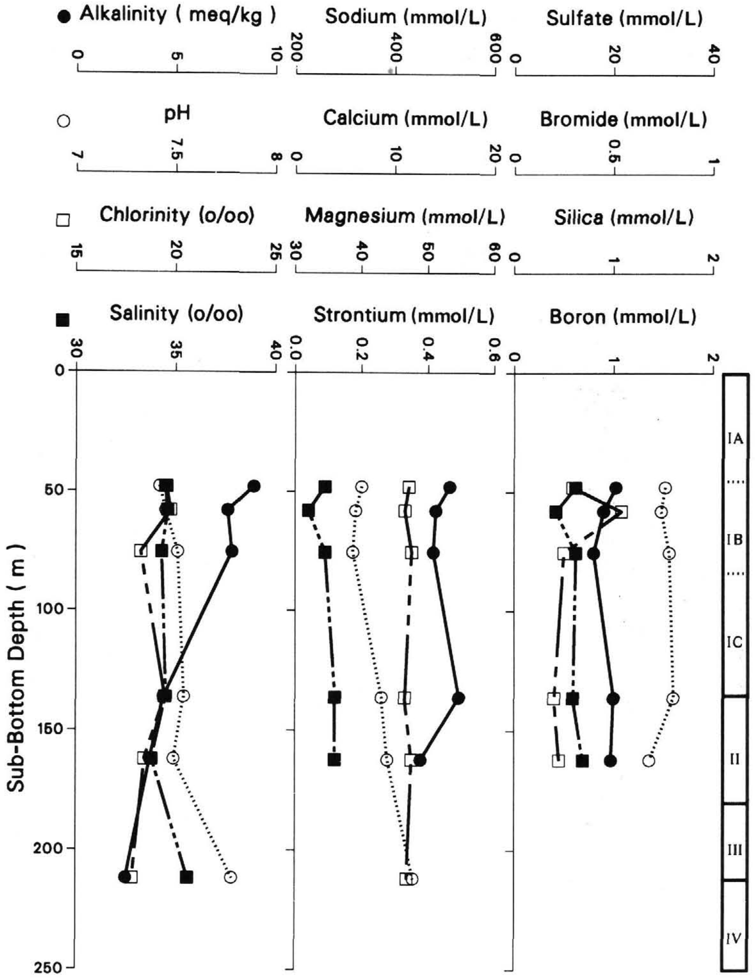

Figure 2. Interstitial-water chemistry, Site 637, plotted against sub-bottom depth and lithologic units.

ganic Geochemistry" section, "Site 637" chapter; Shipboard Scientific Party, 1987a). These non-steady-state conditions have been observed in hemipelagic sections at other Deep Sea Drilling Project (DSDP) sites (Gieskes, 1981, 1983), including Site 400 (Ellis et al., 1979) in the nearby Bay of Biscay.

Site 638 (Fig. 3)

Locality Description

Site 638 was drilled into Lower Cretaceous syn-rift deposits consisting of 248.8 m of sandstone turbidites with interbedded claystone and marlstone (lithologic Unit III), which are overlain by 114.8 m of intercalated marlstone and claystone disturbed by slumping and creep structures (lithologic Unit II). These Cretaceous syn-rift deposits are unconformably overlain by 183.6 m of Neogene (upper Miocene to lower Pleistocene) valley fill (lithologic Unit I). The valley fill sediments are dominantly pelagic. The drill site is midway across a tilted fault block on the outer part of the Galicia margin.

Chemical Profiles

Interstitial-water chemistry profiles at Site 638 are the most complex observed for Leg 103, which probably reflects the complex stratigraphy of the sediments in this region. Alkalinity shows a sinusoidal profile, with two alkalinity maxima. The first maximum is at 167.4 mbsf, just above the top of lithologic Subunit IIA, and appears to be associated with the truncation of the Cretaceous formations that are unconformably overlain by Neogene ooze from Unit I. The second maximum occurs at 443.8 mbsf, in the middle of lithologic Subunit IIB, and may be related to a gradual change from primarily bioturbated nannofossil marlstone to intercalations of claystone turbidites. The second alkalinity maximum is also associated with coarse-grained sandstone turbidites, but the reason for this association is unknown.

The sodium, sulfate, boron, chlorinity, and bromide profiles show two distinct populations. The dividing line between these populations appears to be the unconformity between Cretaceous and Neogene sediments. Above 167.4 mbsf (Unit I), both sulfate and bromide show decreasing trends, whereas sodium and boron are roughly constant. The chlorinity profile is roughly constant to 167.4 mbsf and shows an overall increasing, though erratic, trend below this depth. Below 167.4 mbsf, the distributions for sodium, sulfate, and bromide show a distinct positive shift, and the boron profile begins to drift toward higher values. Sulfate increases to near surface-sediment values. Both boron and bromide increase to above surface-sediment values.

Silica shows erratic behavior, but seems to show a general increase to about a depth of 300 mbsf, where it decreases with depth, which may be related to changes in the solid controlling the dissolved silica concentration. The section becomes more quartz rich in Subunit IIIB (329.9 to 547.2 mbsf).

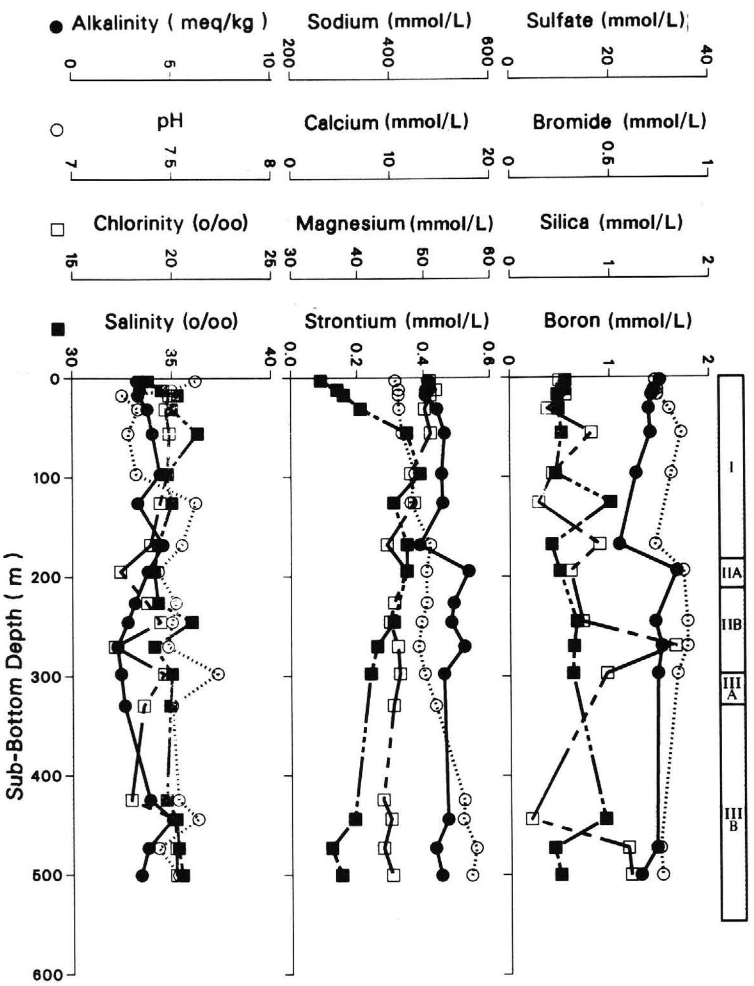

Figure 3. Interstitial-water chemistry, Site 638, plotted against sub-bottom depth and lithologic units.

Overall, the calcium and magnesium profiles are antithetic. Calcium increases with depth whereas magnesium decreases with depth. The calcium profile is more complicated than the magnesium profile and seems to show some of the same characteristics as the alkalinity curve.

Strontium reaches a maximum in Unit I at 96.6 mbsf, and the observed strontium concentrations at and in the vicinity of the maximum are greater by more than a factor of two than strontium concentrations in all other profiles (except for the single strontium observation made for Site 640) for Leg 103. This maximum may reflect recrystallization of nannofossils in the calcareous ooze to form chalk. Strontium concentrations in pelagic microfossils and nannofossils are much greater than those in inorganic calcite reprecipitated from the solution of biogenic calcite (Schlanger and Douglas, 1974; Baker et al., 1982). Recrystallization of pelagic carbonates is usually reflected in interstitial-water chemistry by a distinct strontium anomaly that does not appear to alter the calcium concentration gradient (Hesse, 1986).

The profiles of magnesium, calcium, strontium, and alkalinity appear to be controlled by local sources and sinks and diffusion. Furthermore, the profiles for the alkaline earths do not show a strong response to the unconformity between Cretaceous and Neogene sediments. In contrast, the profiles of sodium, bromide, chlorinity, sulfate, and boron show a marked relationship to the Cretaceous/Neogene unconformity. The chemical data subtly suggest that some of the solutes below the unconformity are derived from evaporated seawater. Sodium, boron, bromide, chlorinity, and sulfate profiles show higher levels of these materials below the unconformity. In addition, the ratio of chloride (from chlorinity data) to bromide shows a general pattern of bromide enrichment with respect to chloride below 157.4 mbsf. This pattern is the expected one for evaporated seawater (McCaffery et al., 1987; Carpenter, 1978; Rittenhouse, 1967). Although no evaporite beds were recovered at any of the sites on this leg, Haggerty and Smith (this volume) report the occurrence of microinclusions of evaporite minerals within the dolomite of the pre-rift strata recovered at Site 639. The contact between the dolomite and the overlying syn-rift calpionellid marlstone was not recovered at Site 639, which is on the same tilted fault block as Site 638. The pre-rift strata at Site 639 are continuous beneath Site 638, where they are covered by rapidly deposited syn-rift sands.

The relationship of sodium, chloride, bromide, sulfate, and boron distributions to the unconformity is highly suggestive of a barrier to ion migration. The lack of such a pattern for the alkaline earths and alkalinity suggests that their profiles are controlled by local sources and sinks.

Site 639 (Fig. 4)

Locality Description

Site 639 penetrated a Jurassic to Lower Cretaceous pre-rift carbonate platform composed predominantly of clayey limestone and dolomite (lithologic Units IV–VI). The carbonate platform is

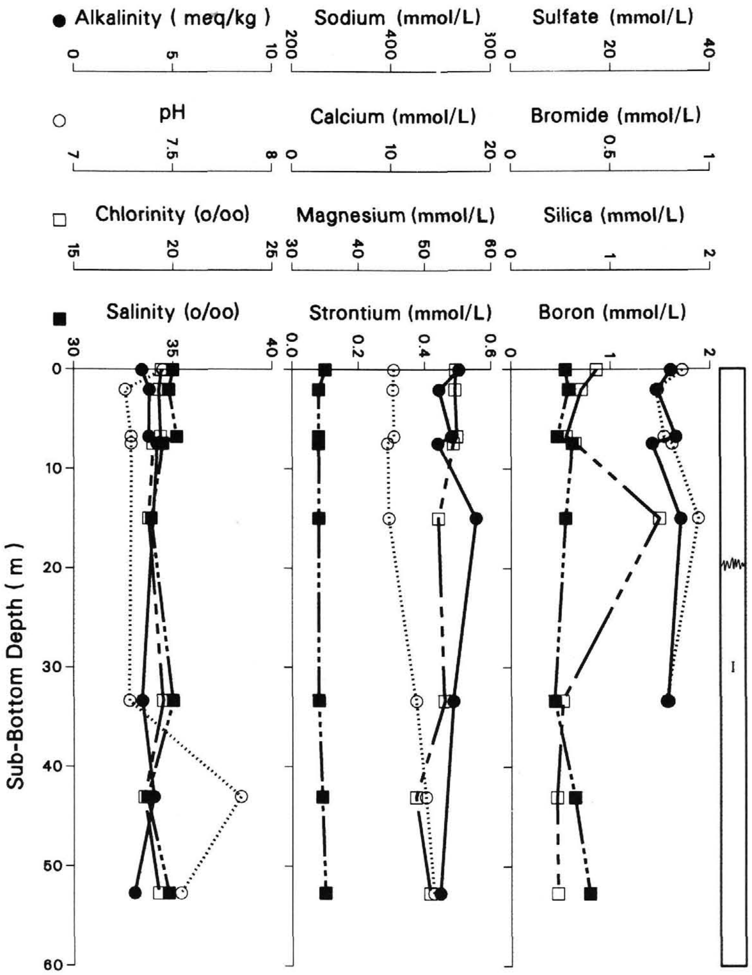

Figure 4. Interstitial-water chemistry, Site 639, plotted against sub-bottom depth and lithologic units.

overlain by Valanginian marlstone (lithologic Unit III), unfossiliferous brown clay (lithologic Unit II), and middle Pliocene to Pleistocene pelagic sediments (lithologic Unit I). The drill site is on the seaward edge of the same tilted fault block that was drilled at Site 638.

Chemical Profiles

Alkalinity exhibits a stable to slightly decreasing trend with increasing depth. Calcium and magnesium show antithetical trends, with calcium increasing and magnesium decreasing. The calcium profile shows a possible increase in slope below about 30 mbsf. The shape of the boron profile replicates that of calcium. The slope change observed in the calcium and boron profiles is coincident with a change from Tertiary to Valanginian marlstone. The profiles of both calcium and boron suggest that the sources for these elements are at depth. In the case of boron, the source may be evaporite dissolution (Collins, 1975). The calcium source may be dolomitization of the marlstone. The lower three samples are from the marlstone in which isolated rhombohedra of authigenic dolomite crystals are observed. Sulfate has a stable to possibly decreasing profile. Silica shows an overall decrease with depth. Profiles of strontium and bromide show little or no change with depth.

Site 640 (Fig. 5)

Locality Description

Site 640 was drilled on the seafloor between the peridotite ridge drilled at Site 637 and the tilted fault block drilled at Sites 638 and 639. At a maximum penetration of 232.2 mbsf, Hauterivian sandstone and marlstone turbidites (lithologic Subunit IIIB) were encountered. These are overlain by Barremian to lower Aptian marlstone and clay ooze (lithologic Subunit IIIA and Unit II), and Paleogene(?) brown clay (lithologic Unit I).

Chemical Profiles

Only two interstitial-water samples were obtained for analysis, from depths of 167.7 and 204.7 mbsf. Both of these samples are from Unit III. The sample from 167.7 mbsf is in Subunit IIIA, which is composed of marlstone and clayey ooze. The sample from 204.7 mbsf is in Subunit IIIB, which is composed of sandstone, limestone, and marlstone microturbidites. These strata are similar to the syn-rift deposits at Site 641. The range of alkalinity and concentrations of magnesium, calcium, silica, sulfate, and bromide observed for these two data points are comparable to those found at similar depths at Site 641 (see "Chemical Profiles" for Site 641). However, the concentration

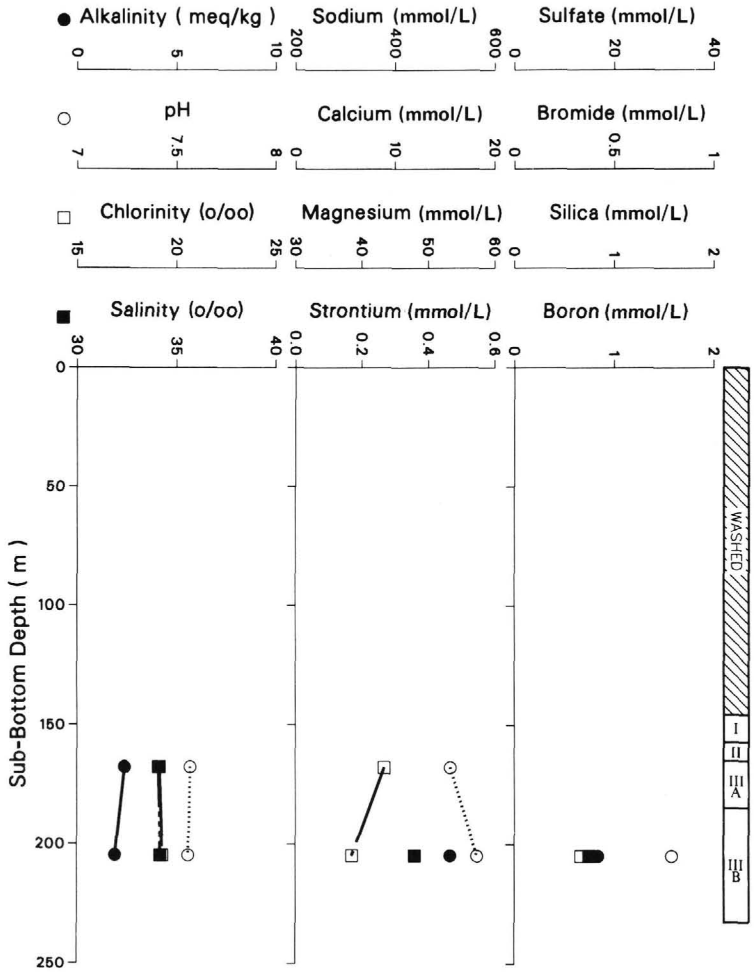

Figure 5. Interstitial-water chemistry, Site 640, plotted against sub-bottom depth. All samples are from lithologic Unit III.

of boron at this site is greater by a factor of approximately 3 than that observed at Site 641. The concentration of strontium is also high (comparable to the highest values at Site 638).

Site 641 (Fig. 6)

Locality Description

Site 641 is located upslope of the tilted fault block drilled at Sites 638 and 639. The deepest sediments penetrated in Hole 641C (maximum depth of 305.2 mbsf) are Barremian marlstone, microturbidites, debris-flow deposits, and calcarenite turbidites (lithologic Unit VI). These sediments are overlain by 32.2 m of Aptian microturbidites and marlstone (lithologic Unit V), 15.7 m of Aptian marlstone and silicified turbidites (lithologic Unit IV), and 51.7 m of Albian claystone (lithologic Subunit IIIB). A large unsampled interval is present at this site between Holes 641A and 641C (63.8 to 150.9 mbsf). Hole 641A bottomed in upper Albian marl (lithologic Subunit IIIA) overlain by 0.03 m of Cretaceous black zeolitic clay (lithologic Unit II) and Paleogene to Upper Cretaceous hemipelagic sediment (lithologic Unit I).

Chemical Profiles

Alkalinity shows no significant variation with depth. The same comment is applicable to the bromide and chlorinity profiles. Decreases in concentration with increasing depth are observed in the profiles of sulfate, boron, and magnesium. In the case of the boron profile, however, there is one excursion at a depth of 219.8 mbsf. The silica profile shows an increase in Hole 641A, but in Hole 641C, the profile is similar to that of the shallowest sample. It should be noted that the minimum silica concentration in Hole 641A is coincident with an outlying boron value. The calcium profile shows a definite increase in concentration with depth.

CONCLUSIONS

Interstitial-water profiles obtained from Sites 638–641 are similar to Hesse's (1986) diffusion-controlled profile for a basin with a low to intermediate sedimentation rate (type I-2). This type of profile is generally characterized by a linear correlation between changes in calcium and magnesium concentration. As shown in Figure 7A, a definite linear relationship exists between the calcium and magnesium concentrations for all sites except Site 637, which shows no relationship between calcium and magnesium. These diffusion-controlled profiles are typical of sediments overlying oceanic crust (McDuff and Gieskes, 1976; McDuff, 1981). The sediments recovered during Leg 103 from Sites 638–641 overlie thinned continental crust (Boillot et al., 1987). These site profiles differ from Hesse's (1986) type I-2 profile in that "crossover" between the increasing calcium and decreasing magnesium profiles is not observed. This may reflect the nature of the alteration reactions between seawater and thinned conti-

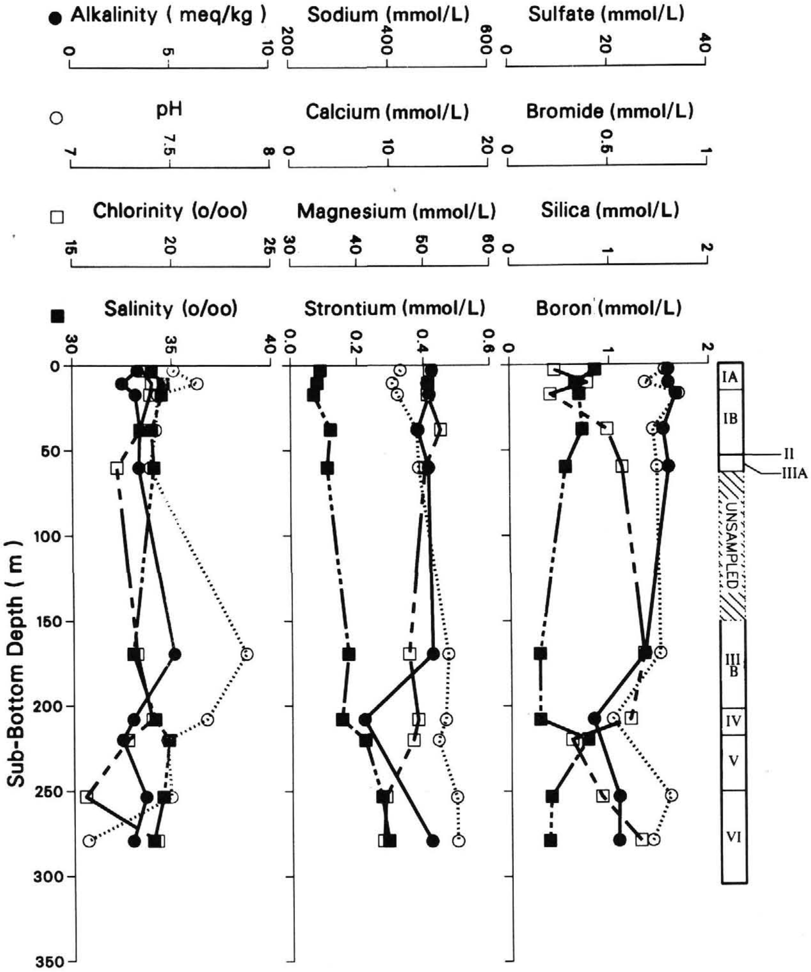

Figure 6. Interstitial-water chemistry, Site 641, plotted against sub-bottom depth and lithologic units.

nental crust at the continental margin; most of the profiles considered by Hesse (1986) were for sediments overlying oceanic crust.

The profiles from Sites 637–641 also differ from the "typical" pore-water profile in that the commonly reported (Hesse, 1986) distinct association between decreasing sulfate concentration and increasing alkalinity is observed in only one Leg 103 profile (Site 638). As shown in Figure 7B, a case might be made for an association between decreasing sulfate and increasing alkalinity for the data set as a whole, but such a relationship is not clearly demonstrated by the sample suites from any Leg 103 site except that from Site 638. This is probably a reflection of the nature of the organic matter present (dominantly type III with some type II), its possibly refractory nature as a consequence of a history of transport and redeposition, and its low abundance (generally <1 wt%) in this sediment-starved continental margin (see "Organic Geochemistry" sections in the site chapters; Boillot, Winterer, et al., 1987). No profile from Leg 103 shows sulfate depletion below 15 mmol/L (approximately 50% of typical seawater). More typical continental margin sediments have organic carbon contents commonly exceeding 2–3 wt% (Hesse, 1986) and usually have low sulfate concentrations at the base of the profiles (Gieskes, 1981, 1983). In addition, the relationship between alkalinity and sulfate may be clouded by lithologic heterogeneity. Sediments encountered at Sites 637–641 range from nearly pure carbonate to brown clay devoid of calcareous biogenic components.

Site 637 does not exhibit the diffusion-controlled profiles of calcium and magnesium described by Hesse (1986) and clearly present (see Fig. 7A) at all other Leg 103 sites. At this site, the amount of magnesium present in the water is decidedly in excess of what would be predicted from all other Leg 103 profiles and bears no obvious relationship to calcium concentration. Basement at Site 637 is serpentinized peridotite. The lack of conformity with the typically observed calcium and magnesium profile relationships is interpreted as being the consequence of alteration reactions with the peridotite basement, which differ in nature from alteration reactions between seawater and either oceanic or continental crust.

The most complete suite of interstitial-water samples came from Site 638 and exhibits the most complex chemical profiles observed on Leg 103. The significant geological control for this chemical complexity is apparently the unconformity between Cretaceous and Neogene sediments. Chemical behavior across the boundary is varied. Calcium, magnesium, strontium, alkalinity, and silica profiles appear to respond to local controls. Sodium, chlorinity, bromide, sulfate, and boron distributions bear a clear relationship to the unconformity, suggesting that the unconformity presents a barrier to chemical migration. The chemical data suggest that some of the solutes present below the un-

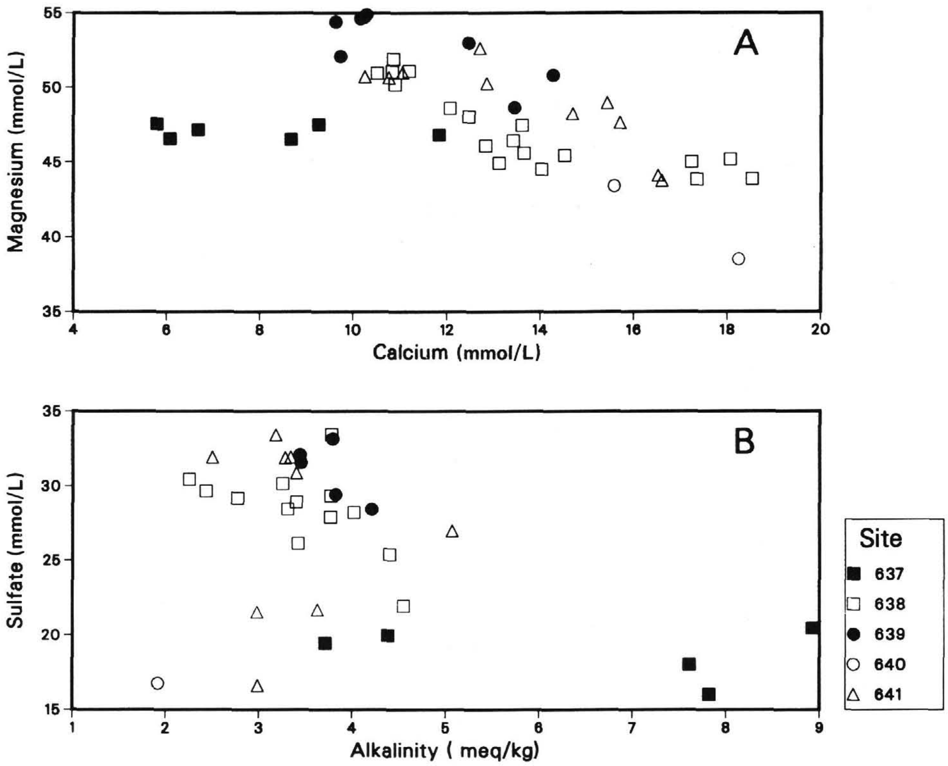

Figure 7. **A.** Calcium and magnesium interstitial-water data from all Leg 103 sites. A distinct relationship in which calcium increases as magnesium decreases exists at all sites, with the exception of Site 637. **B.** Alkalinity and sulfate interstitial-water data from all Leg 103 sites. A distinct association between decreasing sulfate concentration and increasing alkalinity is observed only at Site 638.

conformity at Site 638 are derived from evaporated seawater. The elevated boron levels in the deeper sections of Site 639 may be related to the dissolution of evaporite minerals.

ACKNOWLEDGMENTS

The authors thank Amoco Production Company (Tulsa Research Center) for access to laboratory facilities. We also thank Carl Bennett for his instruction in instrument operation and analytical procedures and the two reviewers provided by ODP for their comments on an earlier version of this manuscript. J. A. Haggerty thanks the Ocean Drilling Program and her shipmates for their help in the acquisition of these samples. This research was supported by a grant from JOI-U.S. Science Advisory Committee.

REFERENCES

Baker, P. A., Gieskes, J. M., and Elderfield, H., 1982. Diagenesis of carbonate in deep-sea sediments: evidence from Sr/Ca ratios and interstitial dissolved Sr^{2+} data. *J. Sediment. Petrol.*, 52:71–82.

Boillot, G., Recq, M., Winterer, E. L., Meyer, A. W., Applegate, J., Baltuck, M., Bergen, J. A., Comas, M. C., Davies, T. A., Dunham, K., Evans, C. A., Girardeau, J., Goldberg, G., Haggerty, J., Jansa, L. F., Johnson, J. A., Kasahara, J., Loreau, J.-P., Luna-Sierra, E., Moullade, M., Ogg, J., Sarti, M., Thurow J., and Williamson, M., 1987. Tectonic denudation of the upper mantle along passive margins: a model based on drilling results (ODP Leg 103, western Galicia margin, Spain). *Tectonophysics*, 132:335–342.

Boillot, G., Winterer, E. L., et al., 1987. *Proc. ODP, Init. Repts.*, 103: College Station, TX (Ocean Drilling Program).

Carpenter, A. B., 1978. Origin and chemical evolution of brines in sedimentary basins. *Circ. Okla. Geol. Surv.*, 79:60–77.

Collins, A. G., 1975. *Geochemistry of Oilfield Waters* (Vol. 1), *Developments in Petroleum Science*: New York (Elsevier).

Ellis, R., Pine, J., and Gieskes, J. M., 1979. Interstitial water studies, Leg 48. *In* Montadert, L., Roberts, D. G., et al., *Init. Repts. DSDP*, 48: Washington (U.S. Govt. Printing Office), 297–303.

Gieskes, J. M., 1974. Interstitial water studies, Leg 25. *In* Simpson, E.S.W., Schlich, R., et al., *Init. Repts. DSDP*, 25: Washington (U.S. Govt. Printing Office), 361–394.

________, 1975. Chemistry of interstitial waters of marine sediments. *Annu. Rev. Earth Planet. Sci.*, 3:433–453.

________, 1981. Deep-sea drilling interstitial water studies: implications for chemical alteration of the oceanic crust, Layers I and II. *In* Warme, J. E., Douglas, R. G., and Winterer, E. L. (Eds.), *The Deep Sea Drilling Project: A Decade of Progress*: Spec. Publ. Soc. Econ. Paleontol. Mineral., 32:149–167.

________, 1983. The chemistry of interstitial waters of deep sea sediments: interpretations of deep sea drilling data. *Chem. Oceanogr.*, 8:221–269.

Hesse, R., 1986. Diagenesis #11. Early diagenetic pore water/sediment interaction: modern offshore basins. *Geosci. Can.*, 13:165–196.

McCaffery, M. A., Lazar, B., and Holland, H. D., 1987. The evaporation path of seawater and the coprecipitation of Br and K with halite. *J. Sediment. Petrol.*, 57:928–937.

McDuff, R. E., 1981. Major cation gradients in DSDP interstitial waters: the role of diffusive exchange between sea water and upper oceanic crust. *Geochim. Cosmochim. Acta*, 45:1705–1713.

McDuff, R. E., and Gieskes, J. M., 1976. Calcium and magnesium profiles in DSDP interstitial waters: diffusion or reaction? *Earth Planet. Sci. Lett.*, 33:1–10.

Rittenhouse, G., 1967. Bromine in oil-field waters and its use in determining possibilities of origin of these waters. *AAPG Bull.*, 51:2430–2440.

Salisbury, M. H., Scott, J. H., et al., 1986. *Proc. ODP, Init. Repts.*, 102: College Station, TX (Ocean Drilling Program).

Schlanger, S. O., and Douglas, R. G., 1974. The pelagic ooze-chalk-limestone transition and its implications for marine stratigraphy. *In*

Hsü, K. J., and Jenkyns, H. C. (Eds.), *Pelagic Sediments on Land and Under the Sea*: Spec. Publ. Int. Assoc. Sedimentol., 1:117–148.

Shipboard Scientific Party, 1987a. Site 637. *In* Boillot, G., Winterer, E. L., et al., *Proc. ODP, Init. Repts.*, 103: College Station, TX (Ocean Drilling Program), 123–219.

________, 1987b. Site 638. *In* Boillot, G., Winterer, E. L., et al., *Proc. ODP, Init. Repts.*, 103: College Station, TX (Ocean Drilling Program), 221–407.

________, 1987c. Site 639. *In* Boillot, G., Winterer, E. L., et al., *Proc. ODP, Init. Repts.*, 103: College Station, TX (Ocean Drilling Program), 409–532.

________, 1987d. Site 641. *In* Boillot, G., Winterer, E. L., et al., *Proc. ODP, Init. Repts.*, 103: College Station, TX (Ocean Drilling Program), 571–649.

Date of initial receipt: 6 May 1987
Date of acceptance: 15 February 1988
Ms 103B-154